# Electromechanical field effects in InAs/GaAs quantum dots based on continuum k→·p→ and atomistic tight-binding methods

Barettin, Daniele; Pecchia, Alessandro; Auf der Maur, Matthias; Di Carlo, Aldo; Lassen, Benny; Willatzen, Morten

*Published in:*
Computational Materials Science

*DOI:*
10.1016/j.commatsci.2021.110678

*Publication date:*
2021

*Document version:*
Accepted manuscript

# Electromechanical field effects in InAs/GaAs quantum dots based on continuum $\vec{k}\cdot\vec{p}$ and atomistic tight-binding methods

Daniele Barettin*
*UNICUSANO, Università degli Studi Niccolò Cusano - Telematica Rome, Italy*

Alessandro Pecchia
*CNR-ISMN, via Salaria Km. 29.300, 00017 Monterotondo, Rome (Italy).*

Matthias Auf der Maur and Aldo Di Carlo
*Department of Electronics Engineering, University of Rome Tor Vergata, Rome (Italy).*

Benny Lassen
*Mads Clausen Institute for Product Innovation, University of Southern Denmark, Alsion 2, Sønderborg (Denmark).*

Morten Willatzen
*Beijing Institute of Nanoenergy and Nanosystems, Chinese Academy of Sciences, National Center for Nanoscience and Technology (NCNST), Beijing 100083, China*
(Dated: May 28, 2021)

A comparison between $\vec{k}\cdot\vec{p}$ and tight-binding methods for the analysis of InAs/GaAs quantum dot bandstructures is presented based on a fully coupled computation of electromechanical effects. Electromechanical effects are addressed using a continuum elastic model for the $\vec{k}\cdot\vec{p}$ method and a pre-conditioned Valence Force Field algorithm for the tight-binding atomistic calculations. The Valence Force Field method allows the direct identification of the impact of internal strain. Results to ensure model parameter consistency between the two methods are also given by comparing bulk and unstrained quantum-well dispersion relations.

The quantum dot size dependence of the bandstructure is investigated based on the models including electromechanical fields. Additionally, the effect of the electromechanical fields is studied for a specific dot size by comparing results with and without electromechanical fields. Good agreement is found for the confined energy levels but model differences show up in the symmetry of probability densities mainly due to the underlying crystal structure details taken into account by the tight-binding method but lacking in the $\vec{k}\cdot\vec{p}$ formalism. The latter follows from not including bulk inversion-asymmetry effects in the $\vec{k}\cdot\vec{p}$ method. Inclusion of piezoelectric field effects in the $\vec{k}\cdot\vec{p}$ method, however, restores the correct symmetry in the $\vec{k}\cdot\vec{p}$ model (in agreement with the tight-binding symmetry).

Results are also given for oscillator strengths where both quantitative and qualitative differences are found in the comparison of $\vec{k}\cdot\vec{p}$ and tight-binding models.

PACS numbers: 68.65.Hb, 77.65.Ly, 31.15.aq

## I. INTRODUCTION

It has been long under debate how accurate the envelope-function approach is in computing electronic bandstructures of quantum-dot structures where some dimensions are down to a few lattice constants[1,2]. Several papers have addressed this topic from different points of view, and in the following paragraph we present a brief overview of the main articles.

The first comparisons between an atomistic pseudo-potential method and 8 bands $\vec{k}\cdot\vec{p}$ model have been given by Wang and co-authors, not including piezoelectric fields[3], and by Zunger[4]. Afterwards, in Ref.[1] the effects of the underlying atomistic structure, atomistic strain fields, and first-order piezoelectric potentials on the electronic structure of zincblende InAs/GaAs quantum dots were discussed in the framework of an atomistic pseudo-potential approach. We can also mention the work of Santoprete et al. on the tight-binding analysis of zincblende InAs/GaAs quantum dots including the effects of an atomistic strain fields on the electronic properties[5]. Finally, a comparison of multiband $\vec{k}\cdot\vec{p}$ models, the effective-bond-orbital approach, and an empirical tight-binding model to calculate the electronic structure for a truncated pyramidal GaN/AlN self-assembled quantum dot with a zincblende structure has been performed, but without including piezoelectric effects[6]. In recent years, several approaches to obtain modern, highly accurate, and fast $\vec{k}\cdot\vec{p}$ models using *ab initio* and experimental results for bandstructure parameters have been suggested[7–9]. These models are suitable for obtaining accurate bandstructures of complicated nanostructure geometries where *ab initio* are computationally too intensive.

The present work contains a numerical study of the relevant InAs/GaAs quantum-dot wetting-layer structures

and a comparison between electronic properties and optical oscillator strengths between a $\vec{k}\cdot\vec{p}$ approach[10] and an empirical tight-binding method (ETB)[11].

This work has been also motivated by a broader perspective of coupling the two methods for a multiscale description of the same structure. For instance the ETB model might be restrained to describe material interfaces where atomistic details are expected to play an important role. Another interesting approach is to include elements of the realistic experimental structure in a multiscale model. Indeed, even if it was argued that in order to reproduce the right symmetry and a correct splitting of energy levels within the $\vec{k}\cdot\vec{p}$ model it is necessary to postulate some unspecified geometric irregularity of the quantum dots[1], more recent articles have indicated that a realistic reproduction of the strain distribution[12] and of the quantum confinement[13,14] of heterostructures can reproduce the same symmetries of an atomistic approach, in excellent agreement with experimental results even in the framework of $\vec{k}\cdot\vec{p}$ model.

In this kind of studies it is crucial to employ reliable $\vec{k}\cdot\vec{p}$ as well as ETB parameterizations, where potential deformations are treated accurately. For this reason we have used well-established methodologies such as the 8 bands ($8\times8$) $\vec{k}\cdot\vec{p}$ model and a 20 bands ($sp^3s^*d^5$ + spin-orbit) ETB parameterization[15]. It is anticipated and expected that the ETB model is superior as compared to the $8\times8$ $\vec{k}\cdot\vec{p}$ model in terms of accuracy as more states as well as an atomistic formulation are used in the former. Early ETB parameterizations based on $sp^3$ or $sp^3s^*$ expansions do not exhibit the same degree of transferability. Furthermore, although articles have been published on parameterization of 14-bands zincblende Hamiltonians[16,17], still full 14-bands $\vec{k}\cdot\vec{p}$ expansions that include reliable deformation potentials are not available.

In the first part of this work we have compared $\vec{k}\cdot\vec{p}$ and ETB bandstructures of strained bulk InAs and GaAs/InAs/GaAs quantum wells (QW) of different lengths. We find that the two methods are consistent in the sense that the band edges and their dependence with strain deformations are in excellent agreement. Also in the QW structures the energy levels of the confined states perfectly converge to the same value above 10 nm. As expected, differences are observed below 5 nm, where the ETB electron states have systematically higher energies. This turns out to be a general trend of the ETB calculations, also observed in the InAs quantum dot (QD) structures.

Only a systematic comparison against precise experimental data might discriminate between the two models, however, such comparisons are always difficult due to uncertainty in dot shape and composition. Furthermore, precise optical data depends on excitonic effects and electron-phonon couplings which are beyond the scope of the present work. For this reason we limit the analysis on spectra and wavefunction symmetries. It was shown by Bimberg et al.[18] using a $\vec{k}\cdot\vec{p}$ model that piezoelectric effects play a dominant role for electronic eigenstates and symmetry properties[19], charge localization in quantum-dot structures and, eventually, oscillator strengths. The latter work employed a semi-coupled model where the piezoelectric potential is due to strain but strain is unaffected by the presence of a piezoelectric potential. While this is usually a reasonable assumption for zincblende structures, the present $\vec{k}\cdot\vec{p}$ work includes piezoelectric effects in a fully-coupled manner[20,21]. ETB results rely on strain input based on, e.g., Keating's Valence Force Field (VFF) atomistic model[22]. The VFF strain results allow the piezoelectric potential to be computed *a posteriori* in a semi-coupled manner. Throughout this work we also show the importance of including the VFF relaxation in conjunction to ETB, since VFF takes into account internal strain and this was found to play a crucial role, especially at material interfaces.

The paper is organized as follows. We begin by presenting the $\vec{k}\cdot\vec{p}$ and ETB models, including a technical discussion about the parameters used and the way strain and deformation potentials are applied. Subsequently, a comparison of the two models applied to bulk and quantum-well structures is given. All models are implemented and solved using the TiberCAD simulator[23,24]. In section IV we present results for different dot structures, comparing the effect of piezoelectric field and deformation potentials. We conclude with the analysis of the optical transition matrix elements based on the dipole approximation.

## II. MODELS

### A. $\vec{k}\cdot\vec{p}$ method

The 8-band $\vec{k}\cdot\vec{p}$ model describes electron, heavy-hole, light-hole, and spin-orbit split-off bands around the $\Gamma$ point of the Brillouin zone and treats all other bands as remote bands. Our $8\times8$ effective-mass Hamiltonian is based on Foreman's application of Burt's exact envelope function theory to planar heterostructures[25,26]. All parameters are taken from Ref.[27]. The wave function of a state $n$ with energy $E_n$ is given by a linear combination of the eight Bloch parts weighted by the respective envelope functions,

$$\psi_n = \sum_{i=1}^{8} \phi_i u_i, \tag{1}$$

where $\phi_i$ are the envelope function and $u_i$ are the Bloch states[28].The $\vec{k}\cdot\vec{p}$ equations were solved with finite elements method (FEM) and inclusion of electromechanical fields is explained in section II C. Within the 8-band envelope function approximation, dipole matrix elements

$\vec{\mu}_{nm}$ are calculated from the momentum matrix element

$$\begin{aligned}\vec{p}_{nm} &\equiv \langle\psi_n|\vec{p}|\psi_m\rangle \\ &= \sum_{i,j=1}^{8}\left(\langle\phi_i^{(n)}|\vec{p}|\phi_j^{(m)}\rangle\delta_{ij} + \langle\phi_i^{(n)}|\phi_j^{(m)}\rangle\langle u_i|\vec{p}|u_j\rangle\right) \\ &\equiv \vec{p}_{nm}^{(\phi)} + \vec{p}_{nm}^{(u)}, \end{aligned} \quad (2)$$

where $\vec{p}^{(\phi)}$ and $\vec{p}^{(u)}$ are the envelope and the Bloch parts of the momentum matrix element, respectively, where the envelope functions are assumed to be slowly varing at the scale of the primitive cell. It is usual to neglect the envelope part[29,30], as this is usually much smaller than the Bloch parts. Oscillator strengths are then given by[31]:

$$\vec{P}_{nm} = \frac{2\pi e^2\hbar^2}{\epsilon_0 m_0^2 V}|\hat{e}\cdot\vec{p}_{nm}|^2, \quad (3)$$

where $\hat{e}$ is the direction unit vector of the electric field of the linearly or elliptically polarized incident light, $V$ is the quantum dot volume, $e$ is the electron charge, $m_0$ is the free electron mass, and $\epsilon_0$ is the vacuum permittivity.

### B. Tight Binding model

The size of realistic quantum dots involves a large number of atoms ($> 100,000$), computationally out of reach for ab-initio approaches, making empirical tight-binding the method of choice in order to obtain accurate single particle eigenstates with atomistic resolution.

Typical ETB methods rely on precomputed parameters for the two-center interactions between atomic orbitals[32]. We use a state-of-the-art ETB parameterization based on a $sp^3s^*d^5$ local basis set given by Jancu et al.[15]. The parameters are fitted to experimental data and accurate DFT bulk dispersions in order to fully reproduce the whole Brillouin zone bandstructure of InAs and GaAs. Spin-orbit coupling is considered within each atomic center as proposed by Chadi[33], making it effectively a 20-band model. Strain fields for ETB are introduced in section C.

ETB optical transitions are described according to the work of Ref.[34], in which momentum matrix elements are evaluated as

$$\vec{p}_{nm}(k) = \frac{m_0}{\hbar}\sum_{b\alpha b'\alpha'} C_{nk}^*(b,\alpha)C_{mk}(b',\alpha')\nabla_k H_{b\alpha,b'\alpha'(k)}, \quad (4)$$

where $n, m$ are eigenstate indices and $b, \alpha$ denotes an atomic orbital $\alpha$ centered at $\vec{R}_b$. In the momentum representation $\vec{\nabla}_{\vec{k}}H_{b\alpha,b'\alpha'(k=0)} = (\vec{R}_b - \vec{R}_{b'})$. In Equation (4) intra-atomic terms and spin-orbit corrections to the transitions are neglected. In the literature, a vivid debate exists as to the correct way of including optical transitions in ETB Hamiltonians. One of the major difficulties is that wavefunctions are not explicitly calculated and dipole matrix elements cannot be evaluated directly. The fundamental works in Ref.[35,36] have shown how to include a Gauge-invariant minimal coupling Hamiltonian to an electromagnetic vector potential based on the Peierls substitution with no additional parameters. One of the draw-backs of the method is that the current-current response function can be easily computed only in one-dimensional structures. The lack of intra-atomic matrix elements can be addressed only extending the original ETB formulation, either by including overlap matrix elements[37] or from constructing effective LCAO wavefunctions[38].

### C. Strain calculations

The models for the calculations of the electromechanical fields are derived following the theory in Ref. [39]. According to the continuum model, the total free energy density change $d\mathcal{U}$ of a piezoelectric medium can be written as

$$d\mathcal{U} = d\mathcal{U}^{mech} + d\mathcal{U}^{elec} = TdS + \sigma_{ik}d\varepsilon_{ik} + E_i dD_i, \quad (5)$$

where $T$, $S$, $\sigma_{ik}$, $\varepsilon_{ik}$, $E_i$, and $D_i$ are the temperature, entropy, stress tensor, strain tensor, electric field, and electric displacement, respectively. Using crystal symmetry considerations with isentropic conditions ($dS = 0$) the energy density of a zincblende structure reads:

$$\begin{aligned}\mathcal{U}^{mech} &= \frac{1}{2}C_{xxxx}(\varepsilon_{xx}^2 + \varepsilon_{yy}^2 + \varepsilon_{zz}^2) \\ &+ C_{xxyy}(\varepsilon_{xx}\varepsilon_{yy} + \varepsilon_{xx}\varepsilon_{zz} + \varepsilon_{yy}\varepsilon_{zz}) \\ &+ 2C_{xyxy}(\varepsilon_{xy}^2 + \varepsilon_{xz}^2 + \varepsilon_{yz}^2) + \mathcal{U}_{ref}^{mech}, \end{aligned} \quad (6)$$

where $C_{ijkl}$ are stiffness constant parameters and $\mathcal{U}_{ref}^{mech}$ is the reference mechanical energy corresponding to an unstrained structure.

These expressions are used to derive the governing equations of the electromechanical fields of the crystal based on Newton's Second Law and Maxwell-Poisson equation[39].

On the other hand, in the atomistic VFF model the free energy $F$[40] is given by:

$$\begin{aligned}F = \tfrac{1}{2}\Big[&\textstyle\sum_{ij} c_1(\delta\mathbf{r}_{ij})^2 + \sum_{ik} c_2(\delta\mathbf{r}_{ik})^2 \\ &+ \textstyle\sum_{BAB} c_3\mathbf{r}_0^2(\delta\theta_{ijk})^2 + \sum_{ABA} c_4\mathbf{r}_0^2(\delta\theta_{jkl})^2 \\ &+ \textstyle\sum_{BAB} c_5\mathbf{r}_0(\delta\theta_{ijk})(\delta|\mathbf{r}|_{ij}) \\ &+ \textstyle\sum_{ABA} c_7\mathbf{r}_0(\delta\theta_{jkl})(\delta|\mathbf{r}|_{jk}) + ...\Big], \end{aligned} \quad (7)$$

where we assume two atoms $A$ and $B$ per unit cell. The first two terms in Eq. (7) correspond to bond stretching forces, $j$ and $k$ denote, respectively, the nearest- and next-nearest neighbors of an atom $i$. The remaining terms represent bond bending forces. Quantities $\delta\mathbf{r}_{ik}$ and $\delta\theta_{ijk}$ represent changes in position vectors and angles from their reference values, respectively. The equilibrium

atomic positions are obtained by minimizing the free energy in Eq. (7).

Previous results clearly indicate that a comparison between the atomistic VFF method and the continuous model shows an excellent agreement for the strain tensors for relatively large dot sizes[39,41].

Continuum-model results are used in the framework of the $\vec{k}\cdot\vec{p}$ as it is usually done via deformation potentials[42].

In ETB calculations, strain effects are taken into account via Harrison-type scaling laws with exponents fitted in order to reproduce strained bulk dispersions[15]. The key ingredient is the atomic positions that can be conveniently calculated by projecting the continuum model (CM) solution described above. However, when scaling down to nanometer-size systems, CM may fail in providing the right symmetries as it lacks a description of the atomistic structure[43]. Moreover, the continuum model does not provide enough information for atomistic methods such as ETB since it cannot accurately capture features at the interfaces and surfaces on an atomistic length scale and, hence, does not provide information on internal strain[40]. The latter was found of fundamental importance in order to obtain physical ETB solutions.

For these reasons the continuum elastic model is used only as a first-order guess to a Keating Valence Force Field relaxation[22] implemented as described in Ref.[44]. The parameters used for the VFF calculations ($\alpha$ and $\beta$) are chosen to ensure consistency with the results of the CM model where, in the latter, elastic constant relations for zincblende crystals are used.

In our ETB scheme, strain also induces an additional tetragonal splitting of the d-levels[45] tuned to biaxially strained quantum-well situations. This correction is important in order to reproduce correct trends of the band edges with strain as shown in Figure 1. An alternative approach, based on overlap corrections of the on-site energies[46], leads to similar results. We extend the approach to quantum dots by considering an average in-plane strain and by noting that the wave-functions are confined within the dots where shear components are negligible and $\varepsilon_{xx} \approx \varepsilon_{yy}$ due to the specific symmetry of the quantum dot shape we have chosen.

The piezoelectric field, included directly in the fully-coupled continuum model, is calculated by a semi-coupled model in the atomistic case as Keating's VFF model does not account for long-ranging Coulomb effects. In an earlier work, it was shown that the differences between the two approaches are negligible for InGaAs zincblende structures (we refer again to Ref.[39] for a detailed discussion).

In order to check the validity of our approach, we tested it for strained bulk structures. In Figure 1, we show the band edges for InAs of conduction and valence heavy-hole, light-hole, and split-off holes at the Γ point as a function of an applied $\epsilon_{xx}$ strain value. The agreement between the two models is excellent in the range considered.

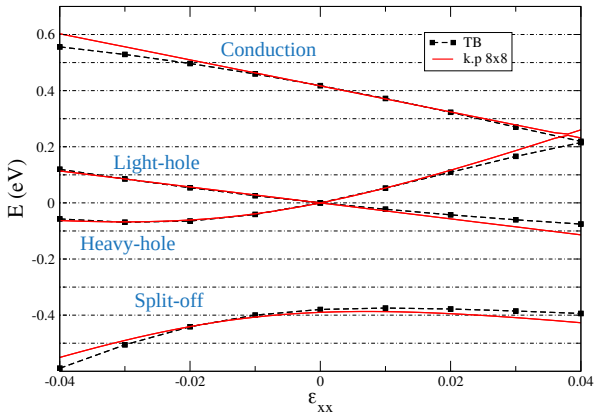


Figure 1: Band edges of InAs for the conduction, heavy-hole, light-hole, and split-off hole bands at the Γ point as a function of $\varepsilon_{xx}$ strain value.

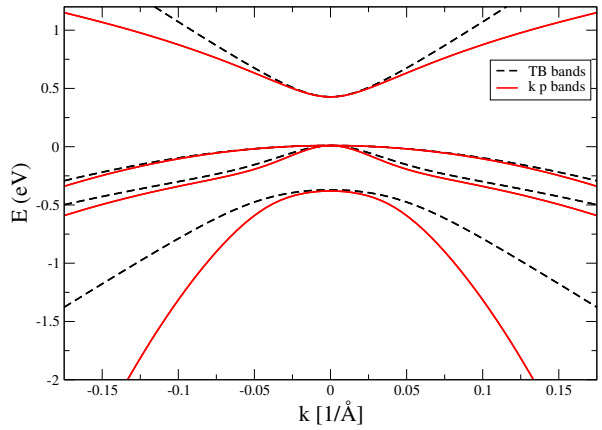


Figure 2: Lower-conduction and upper-valence band dispersion around the Γ point for bulk InAs calculated with the $\vec{k}\cdot\vec{p}$ and ETB methods.

## III. COMPARISON FOR BULK AND QUANTUM WELL STRUCTURES

In order to show that the parameters chosen for the two models are consistent, the bulk and quantum well band structures are studied in this section. In Figure 2, the bulk InAs band structure around the Γ point is shown. From this figure it is seen that a good agreement between the two models is obtained, at least near the Γ point. On the other hand the 8x8 coupling produces a pronounced bowing of the conduction band.

In Figure 3, results are presented using the $\vec{k}\cdot\vec{p}$ and ETB methods for electron and hole ground and first excited state for an unstrained GaAs/InAs/GaAs quantum well as function of the well thickness. We observe that there is an excellent agreement between the hole states, but a considerable discrepancy for the electron states.

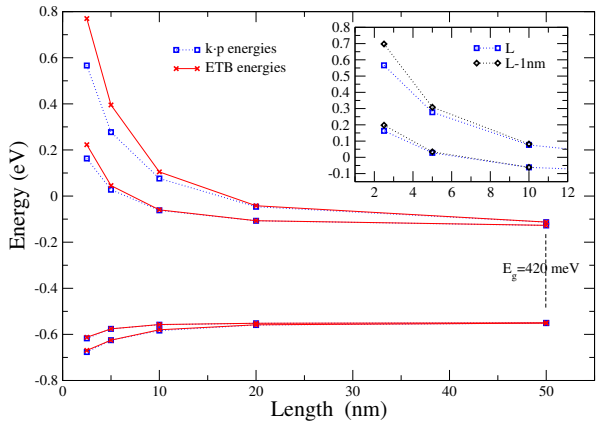


Figure 3: ETB and $\vec{k}\cdot\vec{p}$ electron and hole ground and first exited states in unstrained GaAs/InAs/GaAs quantum wells as function of the well thickness $L$. Insert: $\vec{k}\cdot\vec{p}$ ground and first excited electron states for QWs of length $L$ and $L$-1 nm.

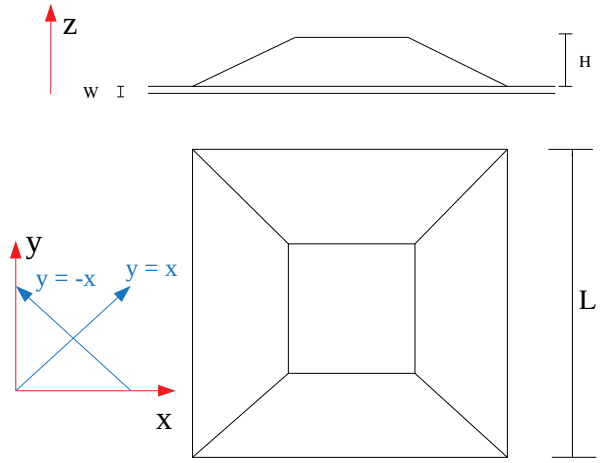


Figure 4: The shape of a zincblende truncated pyramid QD qith the Cartesian axes as implemented in the model.

This energy difference can be understood considering the bulk dispersion shown in Figure 2, since for the shorter well the confined electronic ground state lays at about 0.5 eV above the band edge, where the $\vec{k}\cdot\vec{p}$ dispersion is lower that the ETB band, resulting in a higher effective mass. Additionally, the two approaches treat the confining potential in slightly different ways. In the continuum method there is an abrupt interface, whereas in the atomistic approach a smooth interfaces of about 0.5 nm apply from external Ga atoms to inner In atoms through interface As atoms. This could be interpreted as a variation of the effective length of the QW. In the inset of Figure 3, we see that a decrease in the length of the QW by 1 nm (considering 0.5 nm for the two interfaces) gives rise to energy differences of approximately 50 meV, going in the direction of the ETB energies.

It appears that the hole results for the two models converge towards bulk values at well thicknesses slightly above 10 nm.

## IV. COMPARISON FOR QUANTUM DOTS

### A. Geometry and structure

Results are presented for energies and wave functions of confined states in zincblende InAs/GaAs quantum dots with wetting layer (WL), comparing the $\vec{k}\cdot\vec{p}$ continuum model with the atomistic empirical tight-binding method (ETB). Calculations for the confined states are performed both with and without strain and piezoelectric effect as described in Section II C.

Concerning the shape of the QD, the truncated pyramid that closely resembles experimental shapes of self-assembled Stranski-Krastanov InAs QDs[47,48] has been chosen. The shape and the geometric parameters used in the paper are shown in Figure 4.

Results for QDs of different dimensions are assigned as follows: Dot 1 (the smallest one), Dot 2 (the medium one), and Dot 3 (the biggest one). Dot parameters are specified in Table I. In this work only pure InAs QD have been considered in the comparisons.

| | $L$ [nm] | $H$ [nm] | $W$ [nm] |
|---|---|---|---|
| Dot 1 | 3.0 | 1.0 | 0.5 |
| Dot 2 | 5.0 | 1.5 | 0.5 |
| Dot 3 | 9.0 | 2.0 | 0.5 |

Table I: Quantum dot dimensions.

### B. Comparison without electromechanical fields

In top (bottom) part of Figure 5 the energies of the first three (four) confined electron (hole) states in Dot 3 obtained by the two models are compared. The energies shown do not include strain or piezoelectric effects and all the states are doubly degenerate with respect to spin due to time-reversal symmetry. The first and second excited states are degenerate for electrons (four times degeneracy if we include spin). The energy differences between the two models are around 70 meV for the electrons and 15 meV for the holes.

Following the reasoning of Section III for the QW, both bulk dispersion and volume uncertainty of the QD may explain this energy difference. Indeed, the uncertainty of the exact interface position is compatible with 50 meV energy shifts as $\vec{k}\cdot\vec{p}$ calculations varying the dot size by 0.5 nm give corresponding energy differences of about the same range.

In Figure 6, the probability density $|\psi|^2$ is plotted in a plane normal to the $z$-axis for the electron states corresponding to the energies shown in Figure 5. Similarly,

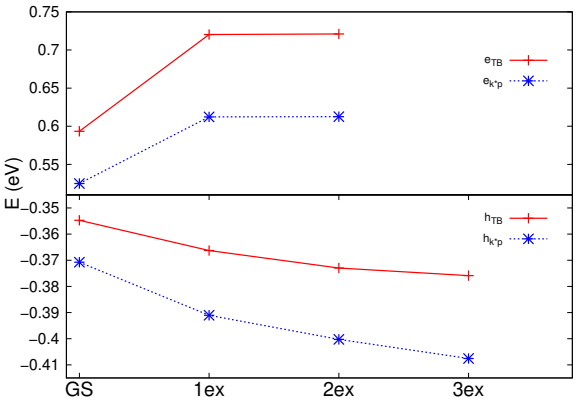


Figure 5: Top: Energies of the GS and the first two excited electron states (1ex and 2ex, respectively) for Dot 3. Bottom: Energies for GS and the first three excited holes states (1ex, 2ex, and 3ex, respectively) for Dot 3. All states are doubly degenerate with respect to spin. Results are for the case without strain and piezo effects.

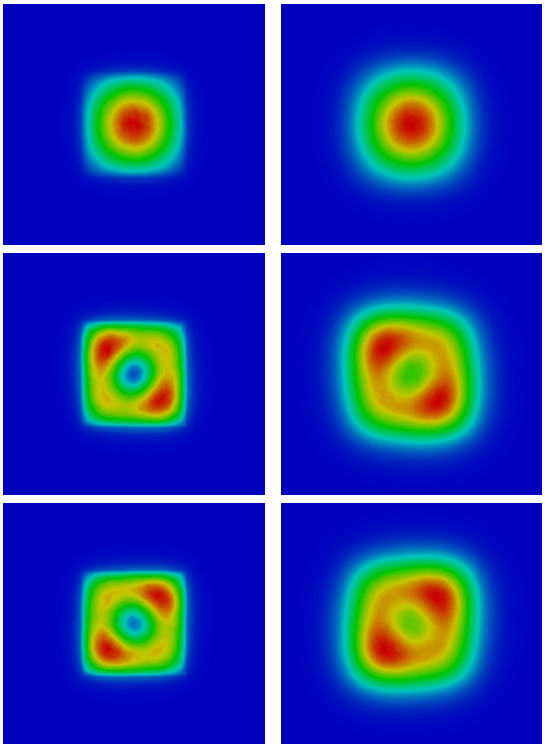

Figure 6: Electron GS (first line), first (second line), and second (third line) excited states for Dot 3 with $c = 1$ in the absence of strain and piezo effects for ETB (right) and $\vec{k} \cdot \vec{p}$ (left).

in Figure 7 the corresponding hole wave functions are shown.

Electronic wave functions of the two models ($\vec{k} \cdot \vec{p}$ and ETB) agree very well, even if the ETB results look less confined as expected from the energy level results. Furthermore, the hole wave functions from $\vec{k} \cdot \vec{p}$ display clearly

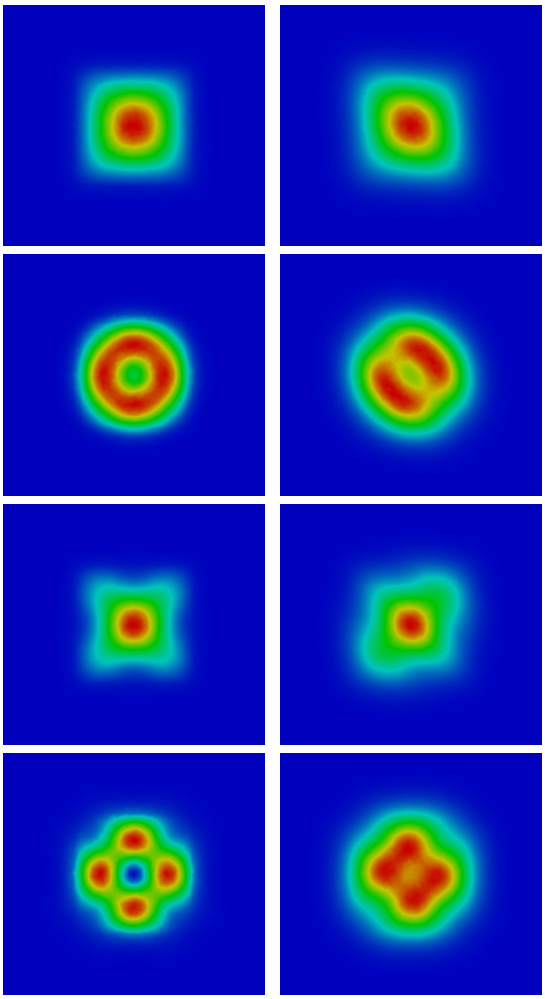

Figure 7: Holes GS (first line), first (second line), second (third line), and third (fourth line) excited states for Dot 3 with $c = 1$ in the absence of strain and piezo effects for ETB (right) and $\vec{k} \cdot \vec{p}$ (left).

the $C_{4v}$ symmetry of the geometric structure, whilst the corresponding states from ETB model reflect the underlying atomistic zincblende crystal structure, i.e., the $C_{2v}$ symmetry.

### C. Comparison with electromechanical fields

In Figure 8, the first few electron and hole energies given by the two models are compared for all three sizes of the QDs including strain and piezoelectric field. Again, due to time-reversal symmetry, all states are doubly degenerate with respect to spin. As in the case without electromechanical fields we can notice that the states found using the ETB model are less confined than the $\vec{k} \cdot \vec{p}$ states and for similar reasons. It is furthermore seen that the general trend in the ground state (GS) is similar for the two models both for electrons and holes. The first two excited electron states are very close in energy for the

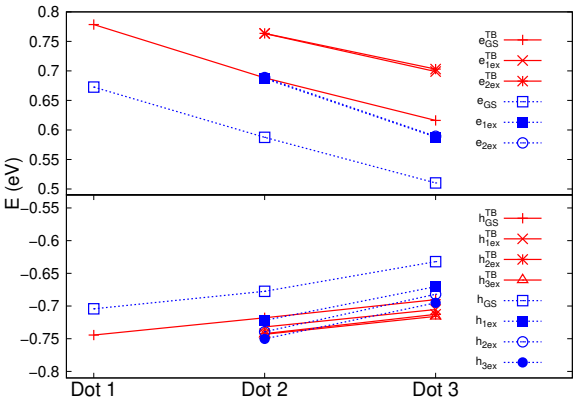


Figure 8: Top: Energies of the GS and the first two excited electron states for the three QDs. Bottom: Energies for the GS and the first three excited holes states for the three QD. All states are doubly degenerate with respect to spin. In both cases the smallest QD (Dot 1) has only one confined state.

$\vec{k}\cdot\vec{p}$ model, while for the ETB model results we observe a slightly larger energy splitting. This has already been found in literature for zincblende GaN/AlN QD[6]. The different slope depends on the lower degree of confinement of the ETB states with respect to $\vec{k}\cdot\vec{p}$. Indeed the ETB states are partially delocalized in the wetting layer.

For the hole excited states the situation is different. It is clearly seen that the excited states found using the $\vec{k}\cdot\vec{p}$ model are further away in energy from the groundstate as compared with the states of ETB . Furthermore, the three excited states of the ETB model are much closer in energy than the corresponding states of $\vec{k}\cdot\vec{p}$, the second and third ETB states being almost degenerate. This result has a strong impact on optical properties. Further, also the hole excited states obtained in the framework of ETB for Dot 2 are quasi-confined states.

In Figure 9, we plot in a plane normal to the $z$-axis the probability density $|\psi|^2$ for the GS and the first two excited states for electrons (Dot 3). The degeneracy between the first and second excited states observed in the models without electromechanical fields is removed since the piezoelectric field favors one of the two possible charge orientations namely the $x=-y$ direction. With the inclusion of strain and related piezoelectricity effects the present model shows $C_{2v}$ symmetry for both ETB and $\vec{k}\cdot\vec{p}$.

It is interesting to observe that our ETB and $\vec{k}\cdot\vec{p}$ methods lead to very similar results for the electronic states qualitatively and quantitatively. We also notice that the ETB states are less confined as compared to the $\vec{k}\cdot\vec{p}$ states. This is in complete agreement with trends seen in the energies plots of Figure 8.

In Figure 10, a behavior similar to what was observed in Figure 9 for electrons is found for the groundstate and the first three excited holes states. However, the favorable orientation of the first excited state is the opposite,

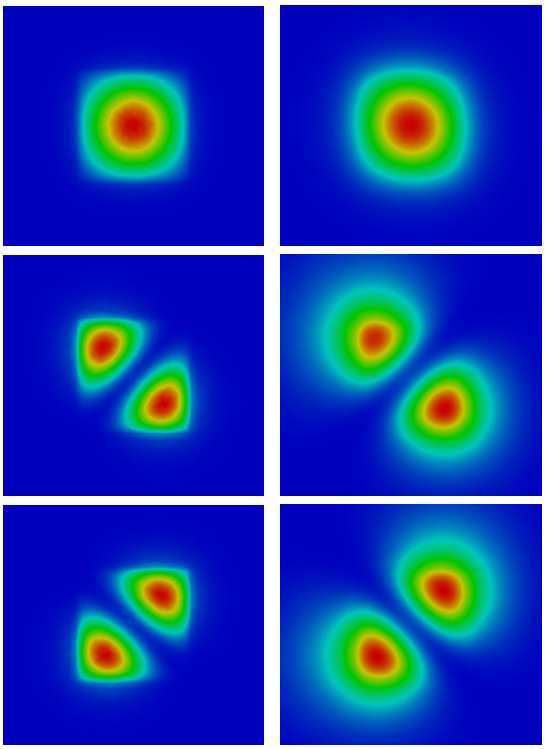

Figure 9: GS (top), first (middle), and second (bottom) excited electron states for Dot 3 with $c=1$ using $\vec{k}\cdot\vec{p}$ (left) and ETB (right) models with electromechanical fields.

$x=y$ due to opposite charges of electrons and holes. Furthermore, it is seen that the states of the ETB and $\vec{k}\cdot\vec{p}$ models have similar symmetries. This is a consequence of the symmetry reduction induced in the $\vec{k}\cdot\vec{p}$ model by the piezoelectric effect.

The necessity to include the VFF algorithm in the ETB calculations, despite the resemblance of the strain tensors of the continuum and atomistic approaches, seems to indicate a remarkable effect of the internal strain on the underlying crystal structure. To stress this, we plot the internal strain on As atoms in the following way: we calculate the strain tensors with CM and we interpolate the results to obtain the atomic positions of the strained crystal structure. Given an As atom in position $r_0$ we define the bond lengths of the strained crystal structure calculated by CM as:

$$d_i = r_i - r_0 \quad \text{with } i=1,..,4, \tag{8}$$

where $r_i$ is the position of one of the 4 nearest neighbors of the As atom. If we now define $d_j$ as the analogous bond lengths given by the calculations of a preconditioned VFF algorithm on the CM results, we can express the standard deviation of the bond lengths after applying the VFF algorithm for every single As atom:

$$\sigma = \sqrt{\sum_{(i\neq j)} \frac{(d_i - d_j)^2}{6}} \quad \text{with } i,j=1,..,4, \tag{9}$$

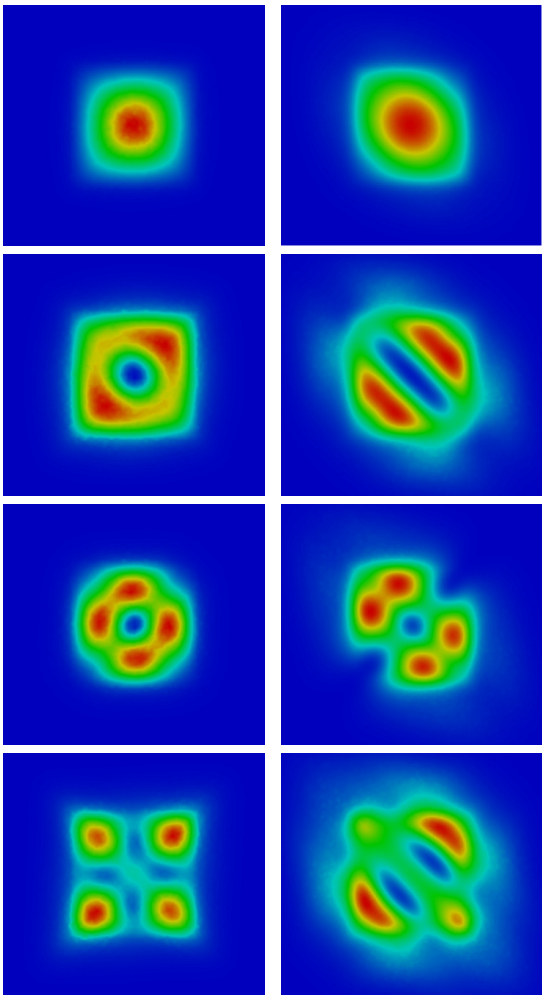

Figure 10: GS (first row), first (second row), second (third row) and third (last row) excited hole states for Dot 3 with $c = 1$ using $\vec{k} \cdot \vec{p}$ and ETB methods, in the first and second column, respectively, with the inclusion of electromechanical fields.

where 6 are all the possible couples of 4 bonds. Now in Figure 11 we plot $\sigma$ on every single As atom on the plane $xz$ both after applying only CM, and after applying VFF as well.

We can see that VFF tends to equalize the bonds, i.e., the difference decreases. However, a gap remains close to the interfaces. This is understandable, because there is an expected deviation of the tetrahedron, since an As atom is linked on one side to 2 Ga atoms and on the other to 2 In atoms. For the relevance of the argument we will present results and analysis of the effects of the internal strain in an independent paper.

In Figure 12, a comparison of the oscillator strengths given by the $\vec{k} \cdot \vec{p}$ and ETB models is shown, both for $P_x$ (identical to $P_y$, due to the symmetry of the wave functions), $P(x = y)$, $P(x = -y)$, and $P_z$ polarized light. Firstly, we notice that there is a general shift in energy peaks between the two models. This is expected (refer

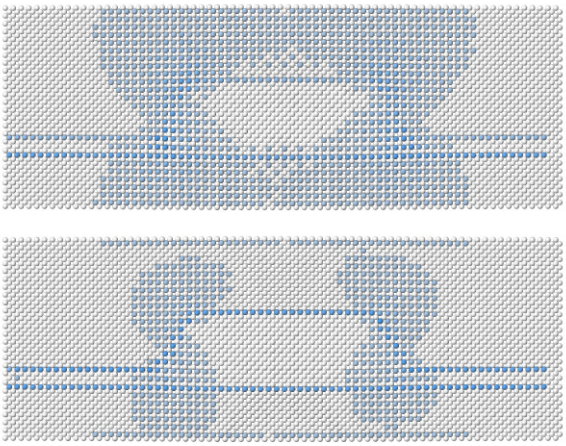

Figure 11: Top panel: standard deviation of the bond lengths after CM calculation on As atoms in $xz$ plane. Bottom panel: the same after VFF. Color scale range between 0 (white) and 0.05 Å(blue).

also to Figure 5) as the energy levels found using the ETB model are less confined than the ones given by the $\vec{k} \cdot \vec{p}$ model. Thus, the transition energies are higher in the ETB case. Secondly, relevant qualitative and quantitative differences between the two models are observed in spite of the similarities in the wave-function symmetries. The larger intensity of the ETB peaks is a direct consequence of larger overlaps between wave-functions.

Concerning $P_x$, the first peak in both spectra corresponds to the transitions between the single particle ground states followed by some smaller peaks associated with transitions between the electron ground state and the first and second excited (also referred to as p-shell in literature) and third excited hole states (d-shell). The hole excited states are more spread out in energy in the $\vec{k}\cdot\vec{p}$ model as compared with ETB results where the states are almost degenerate. The second larger peak in both models correspond to p-shell transitions. While the electron first and second excited states are almost degenerate in both models, the hole first and second excited states are more spaced in energy in $\vec{k} \cdot \vec{p}$ than ETB.

This explains why we clearly see a double peak in the $\vec{k} \cdot \vec{p}$ spectrum, namely given by the transitions between the electron first and second excited states and the hole first and second excited states, respectively. Actually, the same two transitions are possible in the ETB model as well but as they are very close in energy they are not distinguishable in the spectrum.

As expected the inversion asymmetry of piezoelectric charge separation effect induces the anisotropy observed: $P(x = y)$ is different from $P(x = -y)$. In ETB this stems from inversion asymmetry automatically included in the atomistic formulation while the effect in $\vec{k} \cdot \vec{p}$ stems from

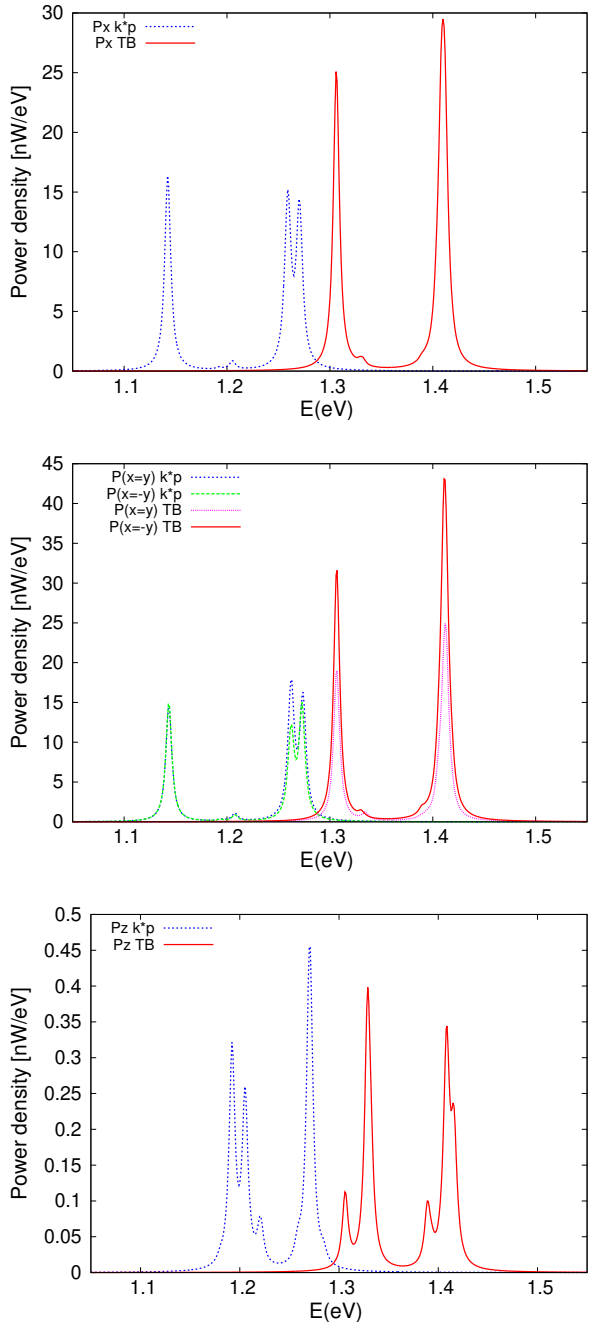


Figure 12: Oscillator strengths given by the $\vec{k}\cdot\vec{p}$ and ETB models for $P_x$ (top), $P(x=y)$ and $P(x=-y)$ (middle), and $P_z$ polarization (bottom).

the additional piezoelectric effect existing solely due to a non-zero strain as our $\vec{k}\cdot\vec{p}$ formulation does not contain bulk inversion asymmetric terms. From the wavefunction plots showed in Figures 9 - 10, it is evident that the $\vec{k}\cdot\vec{p}$ electron and hole *groundstates* are symmetric with respect to reflections in the $x=y$ and $x=-y$ axes hence the GS-GS oscillator strengths $P(x=y)$ and $P(x=-y)$ are the same. In the ETB case, however, the GS-GS oscillator strengths $P(x=y)$ and $P(x=-y)$ are different due to the anisotropy in the hole GS (upper-right plot of Figure 10). For the excited states this symmetry is broken in both $\vec{k}\cdot\vec{p}$ and ETB as Figure 12 reveals.

Finally it is observed that, the peaks corresponding to $P_z$ transitions are considerably weaker than $P_x$ transitions in both models.

## V. CONCLUSIONS

A detailed comparison between $\vec{k}\cdot\vec{p}$ and ETB methods for the analysis of bandstructure of InAs/GaAs quantum dots was given. Electromechanical fields were included in the models by using a fully-coupled continuum model in $\vec{k}\cdot\vec{p}$ while a preconditioned VFF algorithm were implemented for ETB calculations. The importance in using VFF model for atomistic calculations to capture the details of internal strain was demonstrated. To tune model parameters against one another, bulk and unstrained quantum well calculations were carried out.

Results for QDs without electromechanical fields have been obtained for one dot size. A very good agreement was shown for the energy levels trend, while some differences were found for the quantitative values. This can be understood in terms of different interface shapes of the quantum confinement between the two models, i.e., sharp and smooth for $\vec{k}\cdot\vec{p}$ and ETB, respectively. The symmetry of the electron probability densities showed a clear resemblance between the two approaches while the hole probability densities corresponded to a $C_{4v}$ and $C_{2v}$ symmetry for the $\vec{k}\cdot\vec{p}$ and ETB method, respectively, in the absence of electromechanical fields.

Results for QDs, where electromechanical fields have been taken into account, were given for different dot sizes. It was again observed that the ETB energy levels were less confined as compared with $\vec{k}\cdot\vec{p}$ results due to differences in the quantum confinement potentials. The probability densities of both electrons and holes showed similar symmetry for both models as a result of the presence of the piezoelectric field which reduced the symmetry of the system to $C_{2v}$ for both the $\vec{k}\cdot\vec{p}$ and the ETB model.

The oscillator strengths along the $x$ direction displayed both qualitative and quantitative differences, although transitions were of similar magnitude. It was observed that the peak shifts were directly derived from differences in the energy spectrum while the higher values given by ETB model is a consequence of a stronger overlap. The oscillator strengths in the $z$ direction were considerably weaker for both models.

* daniele.barettin@unicusano.it


[1] G. Bester and A. Zunger, Phys. Rev. B 71, 045318 (2005). 1, 2

[2] L. C. Lew Yan Voon, Y. Zhang, B. Lassen, M. Willatzen, Qihua Xiong and P. C. Eklund, J. Nanoscience and Nanotechnology, 8, 1 (2008). 1

[3] L. W. Wang, A. J. Williamson, A. Zunger, H.Jiang, and J. Singh, Appl. Phys. Lett. 76, 3 (2000). 1

[4] A. Zunger, Phys. Stat. Solidi (a), 190, 2 (2002). 1

[5] R. Santoprete, Belita Koiller, R. B. Capaz, P. Kratzer, Q. K. K. Liu, and M. Scheffler, Phys. Rev. B 68, 235311 (2003). 1

[6] O. Marquardt, D. Mourad, S. Schulz, T. Hickel, G. Czycholl, and J. Neugebauer, Phys. Rev. B 78, 235302 (2008). 1, 7

[7] O. Marquardt, M. A. Caro, T. Koprucki, P. Mathé, and M. Willatzen, 101, 235147 (2020). 1

[8] M. Jocic and N. Vukmirovic, Phys. Rev. B 102, 085121 (2020).

[9] C. E. Pryor and M.-E. Pistol, J. Appl. Phys. 118, 225702 (2015). 1

[10] J. M. Luttinger, W. Kohn, Phys. Rev. 97, 869 (1955) 2

[11] W.P. Harrison, *Electronic Structure and the Properties of Solids*, Dover Publications (1989) 2

[12] B. Lassen, D. Barettin, and M. Willatzen, Journal of Physics: Conference Series 367, 012007 (2012). 2

[13] D. Barettin, R. De Angelis, P. Prosposito, M. Auf der Maur, M. Casalboni, A. Pecchia, Nanotechnology, 25 (19), 195201 (2014). 2

[14] D. Barettin, R. De Angelis, P. Prosposito, M. Auf der Maur, M. Casalboni, and A. Pecchia, J. Appl. Phys. 117, 9 (2015). 2

[15] J.-M. Jancu, R. Scholz, F. Beltram, and F. Bassani, Phys. Rev. B 57 (11), 6493 (1998). 2, 3, 4

[16] D. Sytnyk and R. Melnik, arXiv: 1808.06988 (2018). 2

[17] T. Eissfeller and P. Vogl, Phys. Rev. B 84, 195122 (2011). 2

[18] M. Grundmann, O. Stier, and D. Bimberg, Phys. Rev. B 52, 11969 (1995) 2

[19] S. Tomic and N. Vukmirovic, J. Appl. Phys. 110, 053710 (2011) 2

[20] L. Duggen, M. Willatzen, and B. Lassen, Phys. Rev. B 78, 205323 (2008) 2

[21] B. Jogai, J. D. Albrecht, and E. Pan, J. Appl. Phys. 94, 3984 (2003) 2

[22] P. N. Keating, *Physical Review* 145, 2 (1966). 2, 4

[23] TiberCAD Simulation Package (available at: http://www.tibercad.org). 2

[24] D. Barettin, A.V Platonov, A. Pecchia, V.N. Kats, G.E. Cirlin, I.P Soshnikov, A.D. Bouravleuv, L. Besombes,H. Mariette, M.Auf der Maur, A. di Carlo, IEEE J. Sel. Top. Quantum Electron. 19, 1901209 (2013). 2

[25] B. A. Foreman, Phys. Rev. B 48, 4964 (1993). 2

[26] M. G. Burt, J. Phys. Condens. Matter 5, 4091 (1993). 2

[27] I. Vurgaftman, J.R. Meyer, L.R. and Ram-Mohan, J. Appl. Phys. 89, 5815 (2001). 2

[28] E. P. Pokatilov and V. A. Fonoberov, V. M. Fomin and J. T. Devreese, Phys. Rev. B 64, 245328 (2001). 2

[29] A. Schliwa, M. Winkelnkemper, and D. Bimberg, Phys. Rev. B 76, 205324 (2007). 3

[30] D. Barettin, J. Houmark, B. Lassen, M. Willatzen, T.R. Nielsen, J. Mørk, and A.-P. Jauho, Phys. Rev. B 80 235304 (2009). 3

[31] O. Stier, M. Grundmann, and D. Bimberg, Phys. Rev. B 59, 5688 (1999). 3

[32] A, Di Carlo, Semiconductor Science and Technology 18, 1 (2003). 3

[33] D. J. Chadi, Phys. Rev. B 16, 790 (1977). 3

[34] L.C. Lew Yan Voon and L.R. Ram-Mohan, Phys. Rev. B 47, 15500 (1993). 3

[35] M. Graf and P. Vogl, Phys. Rev. B 51, 4940 (1995). 3

[36] T. B. Boykin, R. C. Bowen, and G. Klimeck, Phys. Rev. B. 63, 245314 (2001). 3

[37] T. Sandu, Phys. Rev. B 72, 125105 (2005). 3

[38] M. Zielinski, M. Korkusinski, and P. Hawrylak, Phys. Rev. B 81, 085301 (2010). 3

[39] D. Barettin, S. Madsen, B. Lassen, and M. Willatzen, Commun. Comput. Phys. 11, 797 (2012). 3, 4

[40] P.Y. Yu and M. Cardona, *Fundamentals of Semiconductors - Physics and Materials Properties,* Third Ed., Springer Berlin, (2005). 3, 4

[41] D. Barettin, S. Madsen, B. Lassen, and M. Willatzen, Superlattices and Microstructures 47, 134 (2010). 4

[42] G. L. Bir and G. E. Pikus, Symmetry and Strain-Induced Effects in Semiconductors, Wiley New York, 295, 1974. 4

[43] C. Pryor, J. Kim, L. W. Wang, A. J. Wiallamson, and A. Zunger, J. Appl. Phys. 83, 2548 (1998). 4

[44] M. Auf der Maur, G. Penazzi, G. Romano, F. Sacconi, A. Pecchia, and A. Di Carlo, IEEE Trans. on Elect. Dev. 58, 1425 (2011). 4

[45] J.-M. Jancu and P. Voisin, Phys. Rev. B 76, 115202 (2007). 4

[46] T. B. Boykin, G. Klimeck, R. C. Bowen, and F. Oyafuso, Phys. Rev. B 66, 125207 (2002). 4

[47] C. Cornet, A. Schliwa, J. Even, F. Dor, C. Celebi, A. Ltoublon, E. Mac, C. Paranthon, A. Simon, P. M. Koenraad, N. Bertru, D. Bimberg and S. Loualiche, Phys. Rev. B 74, 035312 (2006). 5

[48] T. Inoue, O. Wada, M. Konno, T. Yaguchi and T. Kamino, Appl. Phys. Lett. 92, 031902 (2008). 5